HHS Public Access

Author manuscript

Biotechnol Bioeng. Author manuscript; available in PMC 2019 January 20.

Published in final edited form as:

Biotechnol Bioeng. 2012 September ; 109(9): 2316–2324. doi:10.1002/bit.24499.

Diffusion-Based Extraction of DMSO From a Cell Suspension in a Three Stream, Vertical Microchannel

Jacob Hanna, **Allison Hubel**, and **Erin Lemke**

Department of Mechanical Engineering, University of Minnesota, 111 Church St. SE, Minneapolis, Minnesota 55455; telephone: 612-626-4451; fax: 612-625-4344;

Abstract

Cells are routinely cryopreserved for investigative and therapeutic applications. The most common cryo-protective agent (CPA), dimethyl sulfoxide (DMSO), is toxic, and must be removed before cells can be used. This study uses a microfluidic device in which three streams flow vertically in parallel through a rectangular channel 500 μm in depth. Two wash streams flow on either side of a DMSO-laden cell stream, allowing DMSO to diffuse into the wash and be removed, and the washed sample to be collected. The ability of the device to extract DMSO from a cell stream was investigated for sample flow rates from 0.5 to 4.0 mL/min (*Pe* = 1,263–10,100). Recovery of cells from the device was investigated using Jurkat cells (lymphoblasts) in suspensions ranging from 0.5% to 15% cells by volume. Cell recovery was >95% for all conditions investigated, while DMSO removal comparable to a previously developed two-stream device was achieved in either one-quarter the device length, or at four times the flow rate. The high cell recovery is a ~25% improvement over standard cell washing techniques, and high flow rates achieved are uncommon among microfluidic devices, allowing for processing of clinically relevant cell populations.

Keywords

diffusion; microfluidic; cell suspension; DMSO extraction; channel flow; cryopreservation

Introduction

Cryopreservation is an enabling technology for a wide variety of fields including cellular therapy/regenerative medicine, biobanking and production of recombinant proteins. Cells that are cryopreserved typically require the introduction of cryoprotective agents (CPA) to provide protection for the cell from the stresses of the freeze–thaw process. The most common cryoprotective agent, dimethylsulfoxide (DMSO), is used at concentrations such that introduction or removal of the solutions, if not done properly, may result in cell lysis (Areman et al., 1990). Additionally, DMSO is toxic to cells and causes negative side effects when infused into patients receiving cell-based therapies. DMSO is typically removed from cell samples by repeated centrifugation and replacement of the supernatant with a wash solution. However, cell losses of 27–30% are typical (Antonenas et al., 2002) due to

Correspondence to: Allison Hubel.

centrifugation and osmotic forces. Automated cell washers reduce labor requirements, but still result in similar cell losses (Perotti et al., 2004).

Microfluidic devices have emerged as a promising method for manipulating cell populations, including cell counting, sorting of heterogeneous cell populations, and controlling exposure to reagents. Devices have separated cells based on size (Huang et al., 2004; Mohamed et al., 2004), fluorescence labeling and deflecting with electromagnetic (EM) fields (Huh et al., 2005), magnetic forces (Pamme and Manz, 2004), acoustic fields (Hawkes et al., 2004; Kumar et al., 2005), and differential cell settling due to gravity (Huh et al., 2007), among other approaches. Microfluidic devices have been used for performing dose-dependent cell assays (Yang et al., 2005), as well as exchanging cell carrier medium (Yamada et al., 2008). This ability to manipulate cells and the chemical environment surrounding them gives microfluidic devices great promise for cryopreservation applications. Extraction of CPAs in microfluidic devices is dominated by diffusion, resulting in gradual shifts in concentration, reducing osmotic stresses on cells when compared to step changes produced by conventional centrifuge-based washing techniques. Cell motion is also typically gentle due to the laminar nature of the flow. Other investigators have used microfluidic devices for introduction and removal of CPA from cell samples which improved cell viability compared to standard protocols, but flow rates were limited to 20 μL/min (Song et al., 2009). Also, most current microfluidic devices handle cell suspensions only at very low cell concentrations (Radisic et al., 2006). In practice, most cryopreservation applications use cell volume fractions (CVF) of 2–20%, and devices would in general need to achieve flow rates of ~1–2 mL/min to be practical. We have previously developed a multi-stage microfluidic device capable of achieving 95% removal of DMSO under these conditions (Fleming et al., 2007; Mata et al., 2008). Each stage of the device consists of a horizontally oriented, rectangular cross-section channel. Two streams flow through the channel in parallel and in contact; a cell- and DMSO-laden sample stream on the bottom, and a PBS wash solution on top. DMSO diffuses from the sample stream to the wash stream, and the two streams are separated at the outlet, thereby removing DMSO from the sample. However, cell recovery from the device is high only under a specific range of flow conditions, restricting the operating window for DMSO removal. The location of cells near the channel bottom also exposes them to significant shear gradients due to the parabolic flow profile, increasing cell losses. Additionally, the device exhibits a significant startup time during which, cell recovery is low due to cells settling into the low velocity flow near the channel bottom (Mata et al., 2009).

This work presents an improved device design, which mitigates many of the cell recovery issues mentioned above while greatly improving DMSO removal. The current embodiment uses three streams flowing downward in parallel through the device. Wash streams are located on either side with a sample (cells and DMSO) stream flowing in the middle. Diffusion-based extraction of CPAs results from the microfluidic environment (short cross-stream distances and laminar flow) established within the channel. Compared to the previous design, the new design increases the interfacial area between streams and shortens diffusion distances, reducing the downstream distance required for removal of DMSO from the sample stream. Cell motion in the device is controlled by placing the cell stream in the center, (the region of lowest shear, and by leveraging gravitational forces to improve cell recovery).

Theoretical Model

Overview of Diffusion Device

A schematic for the three-stream, vertical microchannel is shown in Figure 1 (Glass, 2008b). The device consists of a rectangular cross-section channel 500 μm deep (*y*-direction), 25 mm wide (*z*-direction), and 80 mm long (*x*-direction), through which three streams flow. The center stream contains a DMSO solution with or without cells, whereas the two side streams contain a wash solution. All three streams flow vertically downward (positive *x*-direction) in parallel and in contact with one another within the channel.

Flow within the channel is laminar due to the small cross-stream dimension and low Reynold's number ($Re \sim 2–12$). Therefore, we assume that transport of CPA from the cell-laden stream to the wash streams occurs solely by cross-stream diffusion (*y*-direction), driven by the concentration gradient from the high-concentration cell-laden stream to the lower-concentration wash streams. Cells remain concentrated in the central stream due to their long characteristic diffusion time as compared to a typical CPA molecule as well as low shear gradients in the channel center.

Diffusion Model

The rational design of channel geometry and selection of operating conditions for the device is based upon a theoretical model of the device behavior. The diffusion behavior of CPA within the microfluidic channel can be predicted using a modification of the convection–diffusion equation (Fleming et al., 2007; Glass et al., 2008a; Mata et al., 2008) with the following four assumptions: 1: The flow within the channel is laminar, steady-state, and two-dimensional. The entrance length of the channel is also assumed to be short. Thus the velocity in the channel is in the *x*-direction, and is a function of *y* only. 2: Cells are homogeneously distributed throughout the cell stream fluid, are neutrally buoyant, and move with the local fluid velocity. 3: Diffusion of CPA from the intracellular to the extracellular space can be modeled as a uniform "source" term for the local fluid as cells are small and well dispersed. 4: Based on scaling analysis, diffusion is the dominant mode of CPA transport in the cross-stream (*y*) direction, and convection dominates in the downstream (*x*) direction. Diffusion is negligible in the *x* and *z* directions, and there is no convection in the *y* or *z* directions (Fleming et al., 2007). This results in the following modification of the convection–diffusion equation:

$$v_x \frac{\partial c_t}{\partial x} = \frac{D}{dU}\left(\frac{\partial c_t}{\partial y^2}\right) + \frac{Bd}{U}\left(\frac{V_i}{V_t}\right)(c_i - c_e) \quad (1)$$

where v_x is the local fluid velocity in the *x*-direction, D is the diffusivity of the CPA, d is the channel depth (*y*-direction), U is the average fluid velocity in the channel, c_t is the local extracellular CPA concentration, B is the modeling permeability of the cell membrane to the CPA (membrane permeability divided by membrane thickness. $B = 5$ for this investigation), V_i is the intracellular volume, V_t is the local volume (intracellular and extracellular), and c_i and c_e denote the local CPA concentrations in the intracellular and extracellular spaces,

respectively. The first term captures convection of CPA downstream in the channel. The second term captures the cross-stream diffusion behavior. The third term acts as a source of CPA in the local fluid, and captures the transport of CPA across the cell membrane to the extracellular space.

From Equation (1), three dimensionless parameters become apparent:

$$Pe = \frac{dU}{D} \quad (2)$$

$$B^* = \frac{Bd}{U} \quad (3)$$

$$\frac{V_i}{V_t} \quad (4)$$

Here Pe is the Péclet number, which captures the relative importance of convective to diffusive transport of CPA. For this investigation, $1{,}000 < Pe < 9{,}000$ implying that convection dominates over diffusion in the downstream direction. B^* compares the rate at which CPA is transported from the intracellular space to downstream convection. V_i/V_t represents the portion of the local volume occupied by cells, and hence how much CPA must be transported to the extracellular space before diffusing to the wash streams. Since it is assumed that there are no cells in the wash streams, $V_i = 0$ in the wash streams, and the third term of Equation (1) is dropped.

An additional parameter of interest is the depth fraction, δ/d, or the portion of the channel depth that is occupied by the cell stream. This is related to the volumetric flow rate fraction through the parabolic velocity profile within the channel. The flow rate fraction is defined by (5) where q_c represents the volumetric flow rate of the cell-laden stream and q_t is the total volumetric flow rate through the device (combination of cell and wash streams). The flow rate fraction affects the diffusion behavior in the channel by altering the relative volumes of CPA-laden (cell) and CPA-free (wash) streams, as well as the average distance a CPA molecule must diffuse to exit the cell-stream.

Finally, the Reynolds number, defined by (6), where ρ is the fluid density and μ is the viscosity of the fluid, is of importance for its indication of flow stability within the channel

$$f_q = \frac{q_c}{q_t} \quad (5)$$

$$Re = \frac{\rho U d}{\mu} \quad (6)$$

Computational Model

Equation (1) was solved numerically using a forward-marching finite difference calculation. The solution domain was initialized by setting the entire cell stream to the inlet concentration of CPA and cell volume fraction. Both wash streams were set to zero CPA concentration. No-flux and no-slip boundary conditions were applied at the channel walls. A fully developed parabolic velocity profile was applied throughout the entire domain. The resulting computational model was solved using MATLAB (Mathworks, Inc., Natick, MA).

Experimental Setup and Methods

Figure 2 provides a schematic of the experimental setup. Briefly, a syringe containing the cell suspension (cells + DMSO solution), as well as two additional syringes containing wash solutions (PBS), were driven by a syringe pump, and connected to the device inlets via 3/16 in ID silicone tubing. The three streams flowed in parallel contact through the device, before being separated at the device outlet. Wash stream flow rates were controlled by a second set of syringes being drawn by the same syringe pump. Segments of removable tubing preceding the cell stream inlet and at the wash stream outlets allowed for samples to be taken for analysis. The cell-stream outlet was open to the atmosphere, with samples collected in a vial. Additionally, a microscope and camera were used to observe cell motion within the operational segment of the device.

Flow Control

Volumetric flow rates through the three streams were controlled via a syringe pump (Harvard Apparatus, Inc. Model 22, Holliston, MA). The flow rate for the cell-laden stream was set via the pump controller, and a piston drove the syringe at the desired flow rate (±0.1 mL/min). The same piston was also used to drive the two wash stream input syringes. Because the piston moved all three inputs at the same velocity, the relative volumetric flow rates of the cell stream compared to the wash streams was determined by the relative cross-sectional areas of the syringes. Each of the wash stream inlet syringes was paired with an identical syringe mounted on the reverse side of the piston, such that these reversed syringes drew an equal volume of wash from the outlet as enters the device at the inlet. The cell stream outlet was left open to the atmosphere.

CPA Concentration

The initial concentration used in the studies was 10% DMSO by volume, the concentration used in typical cryopreservation protocols such as those for hematopoietic stem cell products. DMSO concentration in the cell and wash outlet streams was determined by spectrophotometry using methods described in more detail previously (Mata et al., 2008). Concentration was correlated to the sample's absorbance of light at a wavelength of 209 nm, measured using a SpectraMax™ Plus 384 spectrophotometer (Molecular Devices, Inc.,

Sunnyvale, CA). To correlate sample absorbance to a known concentration, a calibration curve was created by serially diluting a sample of stock solution (10% DMSO by volume) over a range of normalized concentrations from $C^* = 1.0–0.0001$ (10–0.001% vol/vol DMSO). Calibration measurements were performed in triplicate for accuracy. The relation between absorbance and concentration is nonlinear. However, it may be approximated as linear for absorbencies ranging from approximately 0.6–1.2 OD (optical density). This region also has a high sensitivity (large change in OD for small changes in concentration).

Samples were taken from the cell stream outlet, as well as both wash outlet streams, for measurement of DMSO concentration. For experiments using cells, the samples were centrifuged to remove cells prior to spectrophotometry. Similar to the calibration curve, samples were serially diluted, in triplicate. Absorbence measurements falling within the linear region of the calibration curve were selected and the actual concentration of the samples was calculated using a fit expression for the linear region as well as the known number of dilutions of the sample.

Cell Motion and Recovery

Cell behavior within the device was investigated using Jurkat cells (lymphoblasts) as a model cell type. Device performance was quantified by tracking cell recovery (Mata et al., 2008) defined as

$$\text{Recovery} = \frac{\text{viability}_{\text{out}}}{\text{viability}_{\text{in}}} \times \frac{\text{CVF}_{\text{out}}}{\text{CVF}_{\text{in}}} \quad (7)$$

where viability is the portion of living cells versus total cells in a sample, and cell volume fraction (CVF) represents the fraction of the sample volume occupied by cells, or a measure of how many cells are in the sample. This measure quantifies both cell losses resulting from cells damaged within the device as well as cells lost to the wash stream or retained in the device. Cell volume fraction was determined using a hemocytometer (Hausser Scientific, Horsham, PA). A minimum of 200 cells were counted for each cell-stream sample. Viability was determined using a membrane integrity dye; a mixture of propidium iodide and acridine orange.

As noted in Figure 2, samples were collected immediately preceding the cell-stream inlet to the device, at the cell-stream outlet, and at the outlets of both wash streams. Samples taken from the cell-stream inlet were used as a reference for device performance. Recovery at the cell-stream outlet measured device performance. Samples taken from the wash-stream outlets were used to determine if cells were being lost to the wash streams, or lingering within the device itself. Also, because the cells are slightly denser than the surrounding fluid, the cells will settle over time. For this reason, samples were taken from the device within 10 min of cell suspension preparation to ensure a homogeneous distribution of cells entering and exiting the device. The cell-stream inlet sample and outlet sample are also separated by less than ~1 mL of fluid (depending on f_q) so time-dependent discrepancies in cell concentration should be minimal.

In addition to tracking cell recovery at various sample locations, cell motion within the device was qualitatively observed using a camera attached to a microscope. The microscope field of view permitted observation of nearly the entire operational segment of the device, from y and z planes.

Results

DMSO Extraction Without Cells

Experiments were performed to characterize the device's ability to remove DMSO from a stream that does not contain cells. DMSO ("cell") stream flow rates were varied from 0.45 to 4.0 mL/min for three flow rate fractions, f_q = 0.15, 0.19, and 0.33. A similar set of experiments was also performed for a single flow rate fraction using a two-stream, horizontally oriented device (used in previous studies), for comparison with the updated device. The DMSO concentration at the device outlet was determined.

Figure 3 shows normalized DMSO concentration, defined as $C^* = C_c/C_o$, where C_c is the "cell" stream concentration and C_o is the original sample concentration, versus the dimensionless parameter $(1/Pe) \times (L/d)$. As described in (Fleming et al., 2007), the extraction behavior of devices of varying aspect ratios collapse to a single curve when plotted versus $(1/Pe) \times (L/d)$, making it useful when considering scaled-up applications of the device. Also, each data point represents the average of a minimum of three separate experiments, with error bars showing one standard deviation. The plotted lines show the outlet concentration predicted by the numerical model, for comparison with experimental values.

DMSO Extraction With Cells

Table I shows the DMSO removal characteristics as a function of cell concentration for the device. DMSO penetrates the cell membrane and therefore must first leave the cells and then diffuse into the wash stream. Studies were performed with Jurkat cells as a model for hematopoietic stem cells with CVFs of 0.5% and 15%. The cells were suspended in a 10% v/v DMSO solution. As with previous experiments, the wash stream consisted of PBS. Experiments were performed with f_q = 0.33 and cell stream flow rates from Q_c = 0.5 to 3.5 mL/min. In Table I, C^* (exp) shows the normalized DMSO concentration at the cell stream outlet as the average ± one standard deviation. C^* (model) is the DMSO concentration predicted by the numerical model for comparison.

Cell Motion

Proper operation of the device requires recovery of a high percentage of the processed cells. Therefore, we investigated the behavior of cells flowing through the device. Images of cell motion were taken from a microscope using 10 × magnification and brightfield illumination. Experiments were performed using f_q = 0.33 and cell stream flow rates between 0.5 and 1.5 mL/min (Pe = 1,263–3,788), with CVF = 0.5%. Images were taken at several locations across the face view (y-direction) to assess the uniformity of cell distribution throughout the cell stream. Figure 4A,C shows representative images near the device inlet and outlet regions, respectively. Image series were also taken from a profile (z-direction) view of the

device, showing the cell and wash streams flowing in parallel. Figure 4,D shows profile-view images also at the inlet and outlet of the device. Scale bars correspond to 115 μm, denoting the width occupied by the cell stream for $f_q = 0.33$.

Cell Recovery

Cell recovery from the device is a critical measure of device performance. Recovery was assessed under a wide range of flow conditions. Figure 5 shows cell recovery versus flow rate for $f_q = 0.19$ and $f_q = 0.33$. The cell stream contained 0.5% cells (v/v) in a 10% DMSO + PBS solution. Cell stream flow rates varied from 0.5 to 3.5 mL/min. As mentioned previously, recovery accounts for the number of cells counted in the sample as well as cell viability. Samples were taken from the cell stream outlet, as well as both wash stream outlets and compared to samples from the device inlet. Recovery from the wash streams denotes cells lost to the discarded wash solution. In Figure 5, each data point is the average of a minimum of three experiments, with error bars depicting one standard deviation.

Figure 6 shows the effect of cell volume fraction on cell recovery from the device. Experiments were performed with CVF = 0.5%, 1.5%, 6%, and 15%. A cell stream flow rate of 2.5 mL/min ($Pe = 6{,}313$) and flow rate fraction of $f_q = 0.33$ were held constant for all experiments in Figure 6. Again recovery was measured at both the cell stream outlet and wash stream outlets. For CVF = 0.5%, 1.5%, and 6%, data points represent the average of three separate trials, with error bars denoting one standard deviation. A single trial was performed for CVF = 15%.

Discussion

DMSO Extraction Without Cells

Figure 3 shows DMSO concentration at the outlet decreases with increasing $(1/Pe) \times (L/d)$. At higher flow velocities (lower values of $(1/Pe) \times (L/d)$) there is less time for DMSO to diffuse from the sample stream to the wash stream before being separated again at the outlet, hence less DMSO is removed at higher flow rates. Also, it can be noted that for each value of f_q, a “removal limit” is approached for increasing values of $(1/Pe) \times (L/d)$. At lower flow velocities, the DMSO continues to diffuse into the wash stream until the concentration gradient becomes negligible. It can also be noted in Figure 3 that for a given value of $(1/Pe) \times (L/d)$, DMSO removal increases with decreasing f_q. This is related to the relative volumes of the wash and sample streams. For lower f_q’s, there is a proportionally larger volume of DMSO-free wash solution to accept DMSO diffusing from the sample stream. The flow-rate fraction also affects the depth ratio, δ/d. Larger values of f_q mean the sample stream occupies a larger width within the channel, δ, and hence the average distance a DMSO molecule needs to diffuse to be removed in the wash stream is larger. The presence of a removal limit, combined with practical limitations on device design, necessitate a multi-stage device to achieve the desired 95% removal of DMSO from the cell sample. Multiple stages of the microfluidic device can be linked in series, passing the sample from one to the next, but introducing fresh wash solution at each stage (Glass et al., 2008a). Figure 3 also shows that the numerical model is in very good agreement with experimental results for

predicting DMSO removal within the device. This behavior is qualitatively very similar to DMSO diffusion in the previous two-stream device (Fleming, 2007; Mata et al., 2008).

Figure 3B shows a comparison of DMSO removal in the current vertical, three-stream device, to removal behavior in the two-stream, horizontal device used in previous studies. The three-stream arrangement increases diffusion from the cell stream to the wash stream by doubling the interfacial area between the streams. Also, the average distance a DMSO molecule must diffuse to leave the cell stream is reduced (Fig. 3B). For a three-stream geometry, the normalized concentration reaches C^*= 0.50 at $(1/Pe) \times (L/d)$ = 0.02, and approaches the removal limit of C^* = 0.33 near $(1/Pe) \times (L/d)$ = 0.10. For a two-stream device under similar conditions, C^* = 0.50 and the removal limit are approached at $(1/Pe) \times (L/d)$ = 0.08 and 0.40, respectively, approximately four times that for the three-stream device. Since the term $(1/Pe) \times (L/d)$ encompasses both length and velocity, this is equivalent to showing the three-stream device can remove the same amount of DMSO as the two-stream, but in either 1/4 of the device length, or at 4× the flow velocity. This allows for either a smaller device size, or faster processing rates, or a combination of the two factors.

DMSO Extraction With Cells

In general, DMSO removal with cells follows trends similar to those without cells, with C^* decreasing asymptotically with increasing $(1/Pe) \times (L/d)$. The presence of cells reduces DMSO removal proportional to the volume of cells present within the sample, as DMSO must first leave the cells before it diffuses from the cell stream. For CVF = 0.5%, the presence of cells causes an increase in C^* at the device outlet of approximately 0.01 according to the model. For CVF = 15%, the effect is more notable, increasing C^* by 0.06. For most flow rates, the experimental results agreed well with the model. However, a significant deviation was noted for the lowest flow rates tested, Q_c = 0.5 mL/min (pe = 1,263). At very low flow rates, C^* is >0.10 higher than model predictions. We believe that this is a result of density differences between the cell-stream and wash-streams. Both the cells and DMSO are denser than PBS, which causes the center stream to settle within the device and may result in deviation of the velocity profile from its standard parabolic shape. A non-parabolic velocity profile implies that the effective Pe for the specific experimental conditions is higher than estimated and therefore the concentration of DMSO at the device outlet will be higher than expected. However, at higher flow rates (Q_c = 1.5 mL/min and higher), the effect becomes less noticeable. As overall flow velocities increase, residence time decreases, allowing less time for buoyancy forces to act. Also, any settling velocity acquired by cells will be comparatively less significant as the overall flow velocity increases. Further studies are needed to confirm the cause of the deviation from model predictions at low flow rates.

Cell Motion

The laminar flow present in microfluidic devices results in favorable motion of cells. The images in Figure 4A,C confirm the cells are uniformly distributed through the x–z plane. Also, in both Figure 4B,D, it can be seen that the cells are largely constrained to the central cell stream where shear forces are minimal and cells do not migrate into the wash streams. Scale bars denote 115 μm, the predicted width occupied by the cell stream assuming a

parabolic velocity profile and for f_q = 0.33. At the device inlet (Fig. 4B) the cells are very concentrated in the center of the device, in a band ~60 μm wide, significantly narrower than the predicted 115 μm. Figure 4D shows the device outlet. Again, cells largely remained in the center, more scattered than at the inlet, and a small portion of cells were observed flowing outside of the predicted 115 mm cell stream. The distribution of the cells in a narrower region of the central stream is consistent with the hypothesis described above (that the velocity profile may not be parabolic across all three streams). Alternatively, if the cells are moving faster than the local fluid, slip velocity may result in hydrodynamic forces repelling cells from the channel walls and moving them towards the center. More detailed studies would be required to determine which factors are responsible for the observed narrowing of the cell-stream.

Image sequences were also used to track cells and approximate their velocities as they pass through the device. Though the accuracy of velocity estimates was limited by camera frame rates, observation of ten cells traveling through the device center showed an average velocity of ~3.6 mm/s. This is faster than the predicted 3.1 mm/s maximum flow velocity assuming a parabolic profile and neutral buoyancy of cells, and reflects the fact that the cells are more dense than the stream in which they are contained and thus settle in the vertically oriented channel. Cells near the channel sides were observed to move slightly slower, at ~3.0 mm/s, due to the presence of a boundary layer near the walls.

Cell Recovery

Cell recovery from the device is a critical measure of device performance. Microfluidic devices have shown promise for cell processing due to reductions in stresses on cells compared to conventional methods. Previous studies with two stream devices (Mata et al., 2008, 2009) have shown cell recovery from the device was high under certain conditions. However, recovery had a dependence on flow rates, potentially limiting the usable flow conditions for the device. Similar restrictions on achievable flow rates with microfluidic devices are a common drawback. One of the goals with the current device was to achieve higher recoveries for a wider range of flow conditions, particularly higher flow rates to increase the clinical applicability of the device. Results in Figure 5 show experiments for two different flow-rate fractions and CVF = 0.5% over a wide range of flow rates. As can be seen, recovery was high, >95% for all flow conditions. At the same time, losses found in wash stream samples were <6% for all cases. This shows that cell recovery from the device is insensitive to flow rate, and does not restrict the usable flow conditions for diffusion or cell processing across the conditions tested.

Studies were also performed at varying cell volume fractions, to investigate limitations on the device's ability to handle a range of cell concentrations. Typical microfluidic devices handle sparsely populated cell suspensions when compared to the 2–20% cytocrits common for cryopreservation. Figure 6 shows recovery results with CVF from 0.5% to 15%. Losses to the wash stream were low (<10%) for all conditions, while recovery was <95%. In some cases, total cells recovered (from both the cell and wash stream outlets) exceeded 100%, which results from the inaccuracies associated with cell enumeration using a hemaocytometer.

High recoveries for a wide range of flow conditions is a marked improvement over previous devices, and particularly over centrifugation cell washing methods. In particular, the ability to handle high CVF samples is rare among microfluidic devices, and helps facilitate processing of clinically-relevant cell populations.

Conclusions

Microfluidic channels have been shown to be an effective option for removal of DMSO from cryopreserved cell suspensions. Changing the device design from a two-stream, horizontal arrangement to a three-stream, vertical device greatly improves device performance, both with respect to extraction of DMSO and recovery of cells from the sample. DMSO removal rate is improved by a factor of four, allowing for either a more compact device, or faster processing flow rates. Though a single device is potentially capable of achieving the desired 95% removal of DMSO, current modeling and studies suggest using several channels in series can shorten processing times and reduce the required volume of wash solution. Further studies are required to determine the optimal device arrangement for DMSO removal. Cell recovery was greater than 95% for all flow rates and cell volume fractions studied. This is an improvement of ~25% over centrifugation washing techniques. Also, results show the device is capable of handling both cell-sparse (CVF = 0.5%) and cell-dense (CVF = 15%) samples at flow rates over 3 mL/min, a flexibility and speed uncommon in most microfluidic devices, providing a viable alternative to centrifugation techniques for processing clinically relevant cell populations.

References

Antonenas V, Bradstock K, Shaw P. 2002 Effect of washing procedures on unrelated cord blood units for transplantation in children and adults. Cytotherapy 4:16.

Areman E, Sacher R, Deeg H. 1990 Processing and storage of human bone marrow: A survey of current practices in North America. Bone Marrow Transplant 6:203–209. [PubMed: 2252961]

Fleming KK, Longmire EK, Hubel A. 2007 Numerical characterization of diffusion-based extraction in cell-laden flow through a microfluidic channel. J Biomech Eng 129:703–711. [PubMed: 17887896]

Glass KK, Longmire EK, Hubel A. 2008a Optimization of a microfluidic device for diffusion-based extraction of DMSO from a cell suspension. Intl J Heat Mass Transfer. 51:5749–5757.

Glass KK. 2008b Numerical modeling of diffusion based-extraction of DMSO from a cell suspension in a microfluidic channel [PhD]. Minneapolis, MN University of Minnesota 138.

Hawkes JJ, Barber RW, Emerson DR, Coakley WT. 2004 Continuous cell washing and mixing driven by an ultrasound standing wave within a microfluidic channel. Lab Chip 4:446–452. [PubMed: 15472728]

Huang LR, Cox EC, Austin RH, Sturm JC. 2004 Continuous particle separation through deterministic lateral displacement. Science 304: 987–990. [PubMed: 15143275]

Huh D, Gu W, Kamotani Y, Grotberg JB, Takayama S. 2005 Microfluidics for flow cytometric analysis of cells and particles. Physiol Meas 26: R73–R98. [PubMed: 15798290]

Huh D, Bahng JH, Ling Y, Wei HH, Kripfgans OD, Fowlkes JB, Grotberg JB, Takayama S. 2007 Gravity-driven microfluidic particle sorting device with hydrodynamic separation amplification. Anal Chem 79:1369– 1376. [PubMed: 17297936]

Kumar M, Felke D, Belovick J. 2005 Fractionation of cell mixtures using acoustic and laminar flow fields. Biotech Bioeng 89:129–137.

Mata C, Longmire EK, McKenna DH, Glass KK, Hubel A. 2008 Experimental study of diffusion-based extraction from a cell suspension. Microfluid Nanofluid 8:457–465.

Mata C, Longmire EK, McKenna DH, Glass KK, Hubel A. 2010 Cell motion and recovery in a two-stream microfluidic device. Microfluid Nanofluid 8:457–465.

Mohamed H, McCurdy LD, Szarowski DH, Duva S, Turner JN, Caggana M. 2004 Development of a rare cell fractionation device: Application for cancer detection. IEEE Trans Nanobioscience 3:251– 256. [PubMed: 15631136]

Pamme N, Manz A. 2004 On-chip free-flow magnetophoresis: Continuous flow separation of magnetic particles and agglomerates. Anal Chem 76:7250–7256. [PubMed: 15595866]

Perotti CG, Fante CD, Viarengo G, Papa P, Rocchi L, Bergamaschi P, Bellotti L, Marchesi A, Salvaneschi L. 2004 A new automated cell washer device for thawed cord blood units. Transfusion 44:900– 906. [PubMed: 15157258]

Radisic M, Lyer R, Murthy S. 2006 Micro- and nanotechnology in cell separation. Intl J Nanomed I:3–14.

Song Y, Moon SJ, Hulli L, Hasan S, Kayaalp E, Demirci U. 2009 Micro-fluidics for cryopreservation. Lab Chip 9:1874–1881. [PubMed: 19532962]

Yamada M, Kobayashi J, Yamato M, Seki M, Okano T. 2008 Milisecond treatment of cells using microfluidic devices via two-step carrier-medium exchange. Lab Chip 8:772–778. [PubMed: 18432348]

Yang S, Undar A, Zahn JD. 2005 Blood plasma separation in microfluidic channels using flow rate control. ASAIO J 51:585– 590. [PubMed: 16322722]

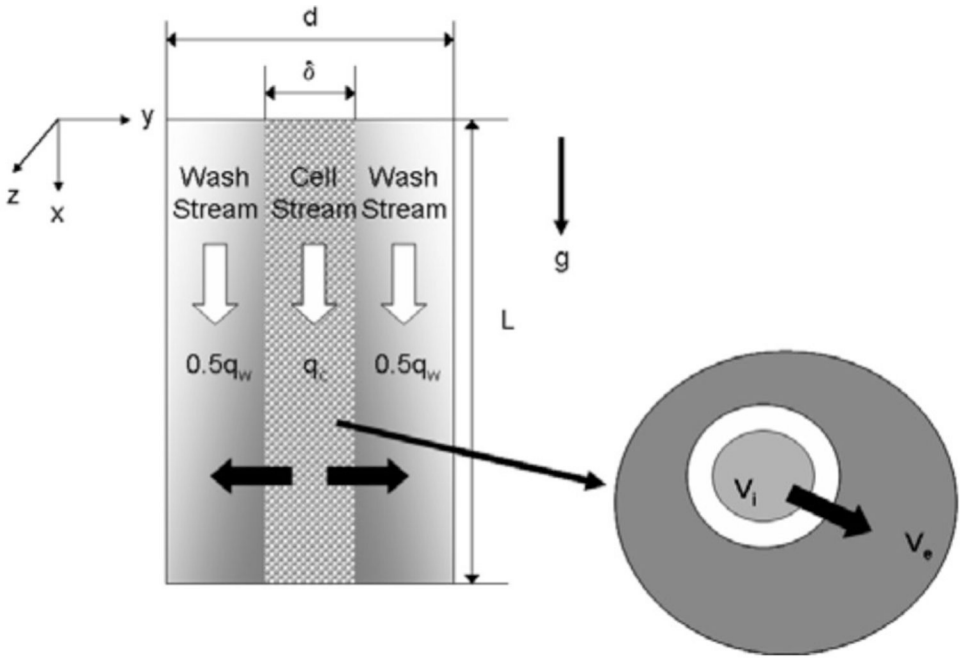

Figure 1.

Schematic of the flow configuration within the channel. A CPA-laden cell suspension flows vertically downward through the center of the channel. A CPA-free wash solution flows in parallel downward on either side of the cell-stream. CPA diffuses from the cell-stream to the adjacent wash-streams. The exploded view depicts transport of CPA across the cell membrane from the intracellular to the extracellular space (Glass, 2008b).

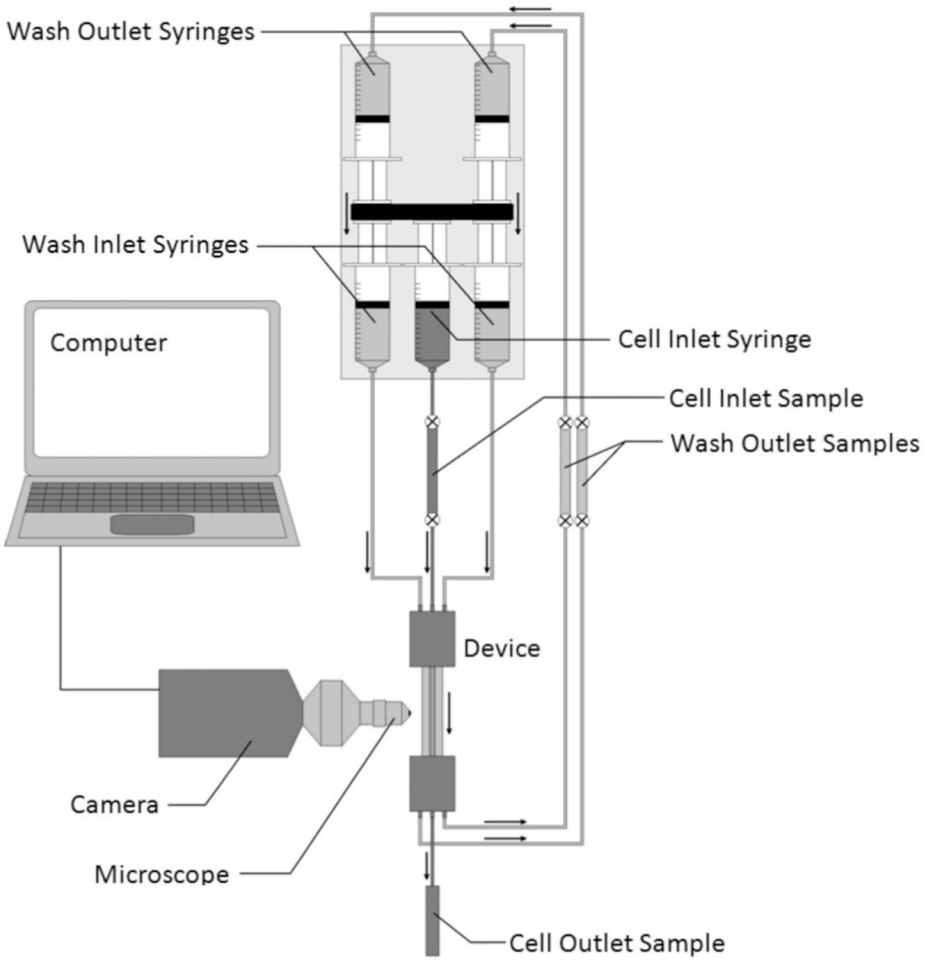

Figure 2.
Schematic depicting the experimental setup, including the device, syringe pump, connections, observational equipment, and sample collection points.

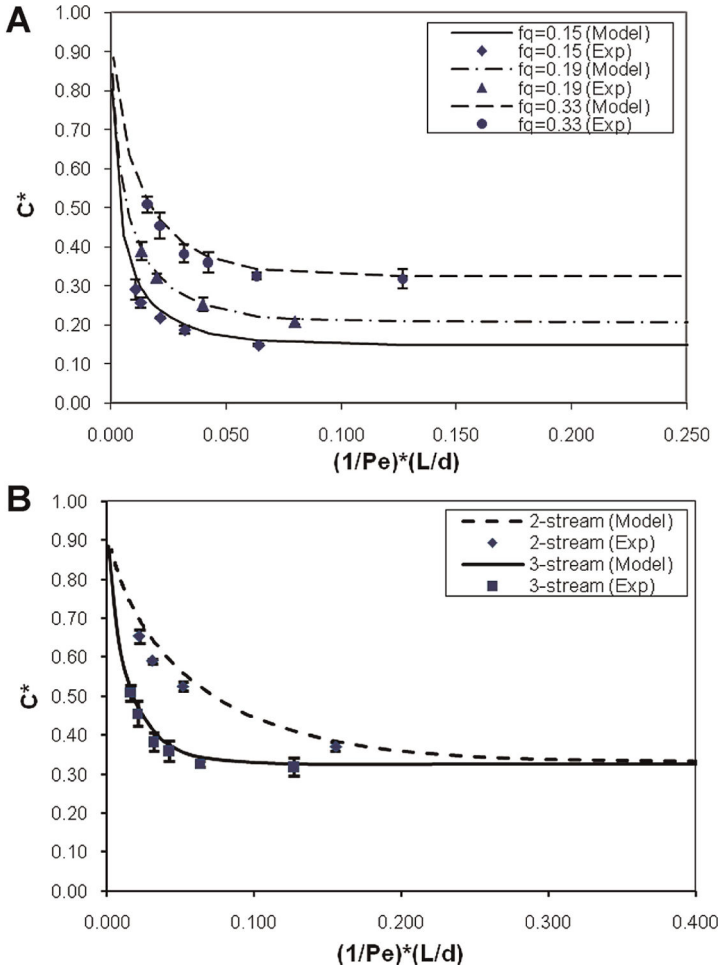

Figure 3.

A: Plot of C^* versus $(1/Pe) \times (L/d)$ showing DMSO removal of the device without cells present. Three different flow rate fractions (f_q) are shown. Curves are also plotted showing the numerical model predictions for DMSO extraction. Each point represents the average of at least three separate experiments, and error bars denote one standard deviation. **B**: Plot of C^* versus $(1/Pe) \times (L/d)$ comparing DMSO removal in the three-stream, vertical device to the two-stream, horizontal device for $f_q = 0.33$. Again lines represent model predictions and each point shows the average of at least three separate experiments. [Color figure can be seen in the online version of this article, available at http://wileyonlinelibrary.com/bit]

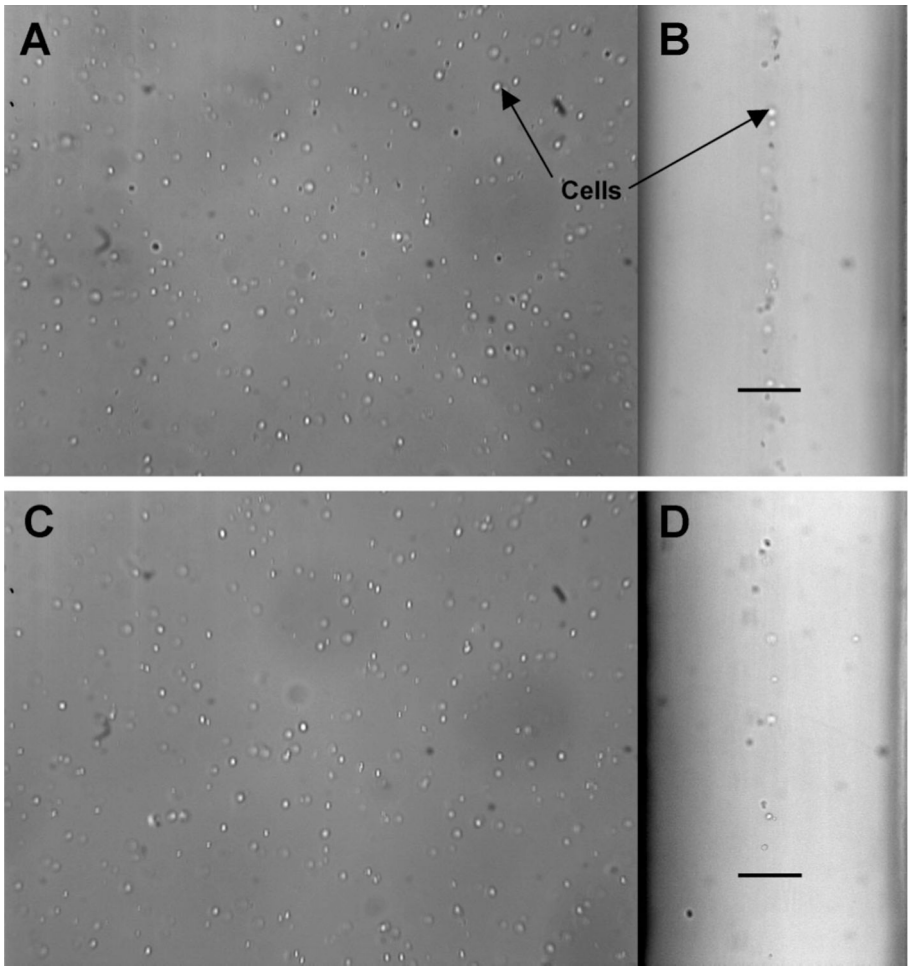

Figure 4.

Brightfield microscope images of cells within the device (10 × magnification). **A**: Face (*y*-direction) view near the channel inlet. **B**: Profile (*z*-direction) view near the inlet showing the cell stream flowing between two wash streams. Scale bar denotes 115 μm. **C**: Face view near the outlet. **D**: Profile view near the outlet.

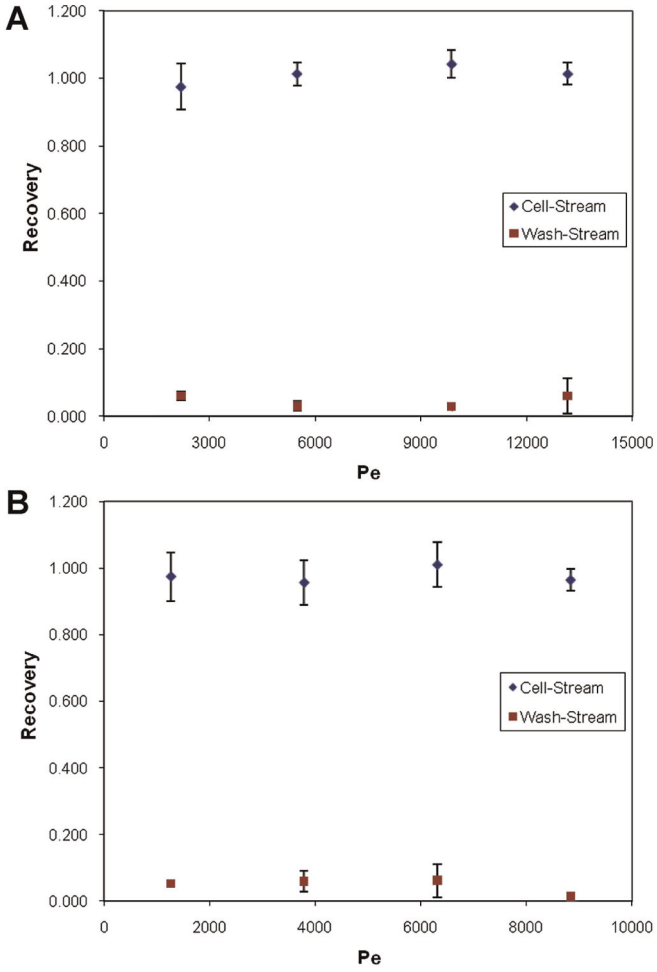

Figure 5.

Plots showing cell recovery from the device for CVF = 0.5%. Results for two flow rate fractions are shown; $f_q = 0.19$ (**A**) and $f_q = 0.33$ (**B**). Cell stream flow rates were varied between 0.5 and 3.5 mL/min. Each data point represents an average of at least three separate experiments, with error bars showing one standard deviation. Samples were taken at both the cell stream and wash stream outlets, to account for cells lost to the removed wash solution. [Color figure can be seen in the online version of this article, available at http://wileyonlinelibrary.com/bit]

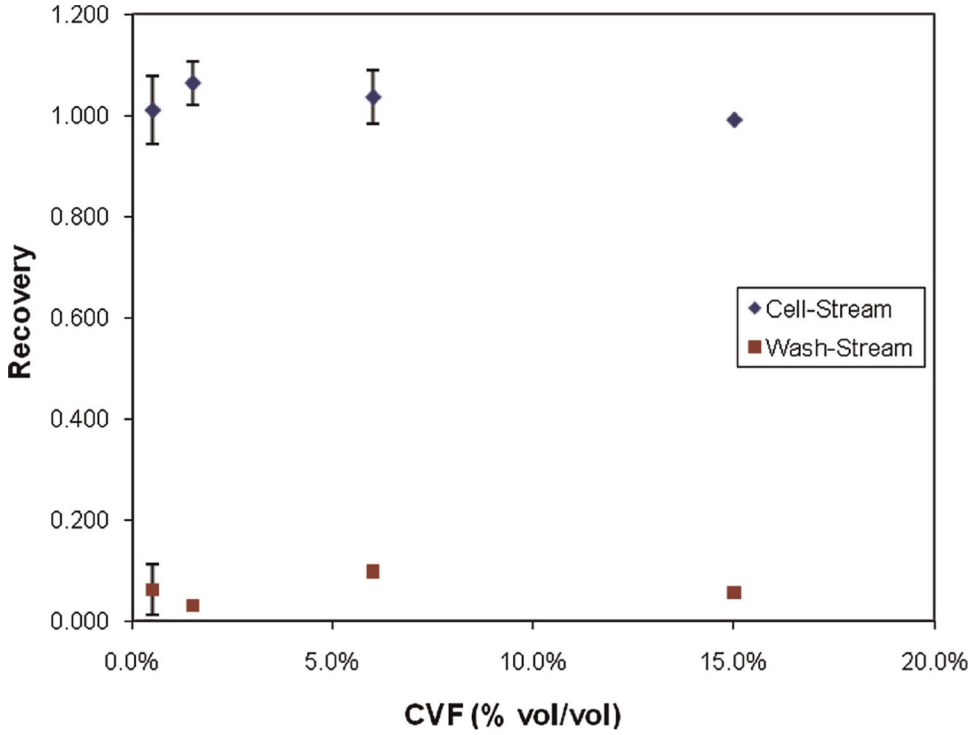

Figure 6.

Cell recovery from the cell stream outlet and wash stream outlets versus CVF. Experiments were performed using Q_c = 2.5 mL/min and f_q = 0.33. For CVF = 0.5%, 1.5%, and 6%, experiments were performed in triplicate, with error bars showing one standard deviation. Results for CVF = 15% represent a single experiment. [Color figure can be seen in the online version of this article, available at http://wileyonlinelibrary.com/bit]

Table I.

Effects of CVF on DMSO concentration at cell-stream outlet for $f_q = 0.33$.

CVF	*Pe*	(1/*Pe*) × (*L*/*d*)	*C** (exp)	*C** (model)
0	1,263	0.127	0.43 ± 0.07	0.33
	3,788	0.042	0.40 ± 0.04	0.38
	6,313	0.025	0.45 ± 0.03	0.44
	8,838	0.018	0.50 ± 0.03	0.50
0.5%	1,263	0.127	0.47 ± 0.09	0.34
	3,788	0.042	0.41 ± 0.04	0.39
	6,313	0.025	0.45 ± 0.03	0.46
	8,838	0.018	0.51 ± 0.02	0.51
15%	1,263	0.127	0.50	0.37
	3,788	0.042	0.48	0.43
	6,313	0.025	0.49	0.50
	8,838	0.018	0.55	0.56

Results for DMSO removal experiments with cells. Experiments were performed with CVF = 0.5% and 15%, as well as acellular experiments. Results show normalized DMSO concentration at the cell stream outlet, as average ± one standard deviation. A minimum of three experiments were performed at each condition for acellular and CVF = 0.5%, and a single trial at each condition for CVF = 15%.